*metals*

MDPI

*Communication*

# Role of Metastable Austenite on Crack Resistance of Quenching and Partitioning Sheet Steels

**Riming Wu *, Yi Xu and Kuicen Li**

School of Materials Science and Engineering, Shanghai University of Engineering Science, 333 Longteng Rd., Shanghai 201612, China

* Correspondence: 05170001@sues.edu.cn; Tel.: +86-21-6779-1202

**Abstract:** The controversial phase, metastable austenite, is deliberately retained in advanced quenching and partitioning (Q&P) sheet steels. Superficially, the plasticity of Q&P steels is enhanced through the transformation induced plasticity (TRIP) effect to a large extent. However, the role of retained austenite on the crack resistance of Q&P sheet steels is ambiguous to date. Tension of double edge notched (DEN) specimens, with different notch radii, was conducted to investigate the role of retained austenite on crack resistance. The fracture toughness of Q&P steels, critical J-integral values Jc, were 402.97 kJ·m$^{-2}$ (notch radius = 0.18 mm) and 584.11 kJ·m$^{-2}$ (notch radius = 1 mm). The increase rate in the plastic deformation zone (PDZ) at notch ahead modeled by finite element (FE) methods dramatically decreased with the notch root radius ρ. It reflects a relatively high sensitivity of notch ductility of Q&P steels in relation to notch radius. Propagating microcracks, regularly initiated at phase boundaries in Q&P steels, were found to be effectively impeded by adjacent retained austenite through energy absorption in the form of strain induced martensite transformation (SIMT).

**Keywords:** quenching and partitioning (Q&P); transformation induced plasticity (TRIP) effect; double edge notched (DEN) specimen; fracture toughness; strain induced martensite transformation (SIMT)



**Citation:** Wu, R.; Xu, Y.; Li, K. Role of Metastable Austenite on Crack Resistance of Quenching and Partitioning Sheet Steels. *Metals* **2023**, *13*, 762. https://doi.org/10.3390/met13040762

Academic Editors: Di Yun and Filippo Berto

Received: 9 March 2023
Revised: 30 March 2023
Accepted: 31 March 2023
Published: 14 April 2023



## 1. Introduction

Metastable austenite containing quenching and partitioning (Q&P) [1] attracted interest from experts researching advanced high strength steels for automobile use [2–4]. A partitioning treatment was significantly included in Q&P treatment to partition the excess carbon in martensite to retained austenite (RA), so the start temperature of martensite (Ms) of RA was reduced to a temperature below the ambient temperature. The stability of RA is of utmost significance for toughness [5]. Several factors were ascribed to effectively tailoring the stability of RA, e.g., size [6,7], morphology [8], composition [9,10], location [8–11], etc.

Improved uniform elongation was achieved by the transformation induced plasticity (TRIP) effect, which effectively relaxes the stress concentration [12–14] as well as redistributes residual stress [15]. Metastable austenite was proved to effectively take effect in enhancing the fracture toughness [11]. In the deformation of metastable austenite containing steels, severe notch sensitivity would lead to premature damage [16], which was correlated to the fracture toughness J-integral [17]. The J-integral indicates the capacity of a component to resist nucleation and the growth of internal voids [18]. It means the energy dissipates locally at the crack ahead during necking.

Recently, a 0.20%C-1.51%Si-1.52%Mn-1.03%Cr-0.05%Nb-Fe (balance) (in mass %) TRIP-aided steel was reported [18] with ultrahigh fracture toughness $K_{IC}$ = 129~154 MPa·m$^{1/2}$ because of fine metastable RA. Qiu et al. [19] drew a conclusion that strain induced martensite transformation (SIMT) not only enhances the fracture toughness but also changes the fracture mode. The crack growth rate was evidently slowed down, and it was attributed to shielding and blunting effects at the crack tip [20]. The closure of crack was subjected to the

roughening of the crack surfaces and compression stress from adjacent structures [21,22], with the aim to investigate the notch sensitivity and fracture toughness during deformation [23,24] of novel high strength Q&P sheet steel. A double edge notched (DEN) specimen is applied for fracture toughness measurements, and the geometry can be seen in the author's original work [14]. The DEN specimen was applied for the determination of $J_{IC}$ and crack tip opening displacement of TRIP steel [16–25]. A finite element simulations method [25] was conducted to testify the validity.

In this work, the fracture toughness of novel Q&P steel, critical J-integral values Jc, was measured using DEN tension tests. Elastic–plastic finite element simulations of DEN tension tests were performed to assess the notch sensitivity. After a description of the materials (Section 2.1), experimental procedure (Section 2.2) and numerical procedure (Section 2.3), Section 3 will present the experimental and numerical results and the discussions. Section 3 will focus on (I) notch sensitivity of Q&P steel (Section 3.1), (II) the role of RA in fracture toughness (Section 3.2), (III) the transformation induced plasticity (TRIP) effect of RA (Section 3.3) and (IV) the SIMT effect of RA (Section 3.4).

## 2. Materials and Experimental Procedures

### *2.1. Materials*

The composition of Q&P steels was C (0.20 wt.%)—Si (1.42 wt.%)—Mn (1.87 wt.%)—Al (0.0405 wt.%)—Fe (balance). It was composed by 8 vol. % RA, 61 vol. % ferrite and 31 vol. % martensite. The measured ultimate tensile strength, yield strength and total elongation were 886 MPa, 458 MPa and 27%, respectively.

### *2.2. Experimental Procedures*

Notched sensitivity test: DEN specimens (Figure 1) were rectangular plates with a size of 1.2 mm (thickness) × 45 mm × 90 mm. A finite tip radius ρ was machined at the edge of the notches. Different notch root radii were machined (ρ = 0.18, 0.5, 1, 2 and 5 mm). The DEN specimens with a notch root radius of 0.18 and 1 mm were designated as "DR0.18" and "DR1", respectively. Tension tests were conducted on DEN specimens. Three specimens for each notch root radius were evaluated.

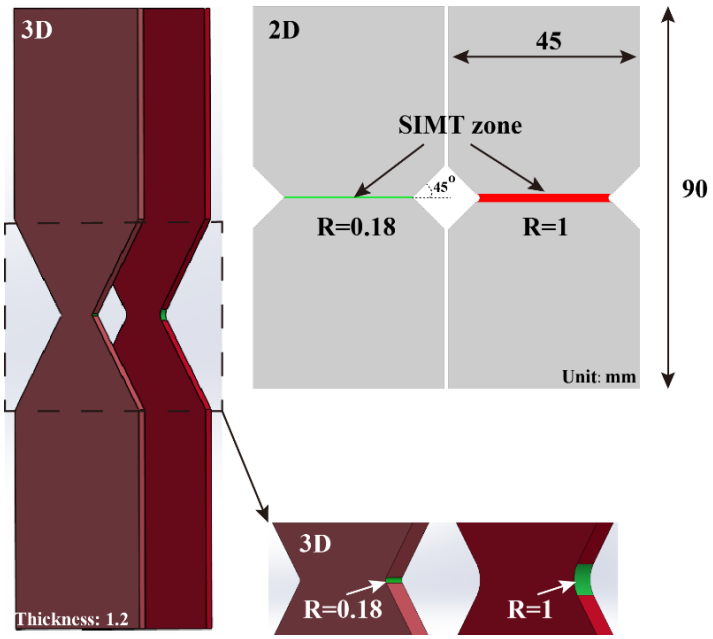


**Figure 1.** Specimens of DEN tension with notch radii of 0.18 mm and 1 mm. SIMT indicates strain induced martensite transformation.

Fracture toughness test: After the DEN specimens were pre-cracked on a fatigue testing machine [26], the tension tests on the DEN specimens were interrupted at different load stages. J-integral and the crack advance, Δa, were both recorded. Finally, the cracking resistance of the $J_R$ curves was calculated from the load versus displacement curve [17]:

$$J = \frac{K_I^2}{E} + \frac{1}{l_0 t_0}\left(2\int_0^{U_p} P(u_p)du_p - PU_p\right) \quad (1)$$

$K_I$, $E$, $u_p$, $P(u_p)$ and $U_p$ indicated mode $I$ stress intensity factor, Young's modulus, plastic displacement, load and the maximum plastic displacement, respectively. Based on the relationship between the $J_R$ and notch radiuses, the critical value of toughness Jc can be deduced when the notch radii is close to zero [27].

Before the SEM observation, the steel samples were cut by EDM, followed by grinding, polishing and etching using 4 vol. % Nital solution. Field emission gun scanning electron microscope (SEM, S3400-N, Hitachi, Japan) observation was performed on the Q&P steels operating at 15 kV. After the SEM observations, the steel samples were subjected to polishing, followed by electropolishing in perchloric acid (8 vol. %) alcohol solution. Electron back-scatter diffraction (EBSD, Zeiss ULTRA-55, Oxford Instruments, Abingdon, UK) and X-ray diffraction (XRD, PANalytical X' Pert Pro, Almelo, The Netherlands) measurements were both conducted. EBSD operated at 20 kV (step size: 0.03–0.08 μm). EBSD data were processed by AZtec and HKL CHANNEL5 software (Oxford Instruments, London, UK).

Through a direct comparison of the integrated intensity of (200) $_\gamma$, (220) $_\gamma$ and (311) $_\gamma$ with (200) $_\alpha$ and (211) $_\alpha$ peaks [28], the levels of RA in the samples without tension were calculated by XRD with Cu-Kα radiation (D/max-2550 X-ray diffractometer) [29]. After tension of the DEN specimens, square specimens at the notch tip with a size of 3 mm × 3 mm × thickness (thickness of the Q&P sheet steel) were cut down, and the level of RA ($f_\gamma$) at the crack front was intermittently measured using magnetic methods [30].

### *2.3. Numerical Procedures*

An elastic–plastic finite element (FE) model of a tensile test was constructed to predict the evolution of a plastic deformation zone (PDZ) under a certain strain [14] using the commercial code DEFORM™ (Version 10.2, Science Forming Technology Corporation, Columbus, OH, USA). Furthermore, 18,880 and 6840 were determined as the total numbers of nodes and elements, respectively. Finally, 0.1 mm/s of velocity was set as the boundary conditions on both sides of the DEN specimen.

## 3. Results and Discussion

### *3.1. Notch Sensitivity*

Metastable austenite of Q&P steel is an extra phase, which would affect the evolution of PDZ distribution as strain. As novel Q&P steel was applied to structural components with notches, notch sensitivity is an utmost issue to be classified.

Figure 2a–c show the engineering stress versus axial displacement curves of DEN tension on Q&P steels. The occurrence of large stress concentration in the vicinity of the notches diminishes the outstanding properties of Q&P steels. The color bars under the curves (Figure 2a,b) indicate the effective strain level. Effective strain superior to 0.067 is underlined, and the zone with effective strain superior to 0.067 is totally marked using a red color, and the others are marked using a grey color. As axial displacement increases, the PDZ firstly initiates at notch ahead, followed by the formation of circular PDZ, and then PDZ grows to the region outside. Comparatively, the volumes of PDZs in DR1 increased slower than those of DR0.18. The PDZs distributions by FE were in line with previous findings [14]. Compared with the standard tension of Q&P steel, the DEN tension of Q&P steels appeared highly sensitive to notch as well as axial displacement. The volumes of PDZs in Q&P increased remarkably as the radius of the notch decreased.

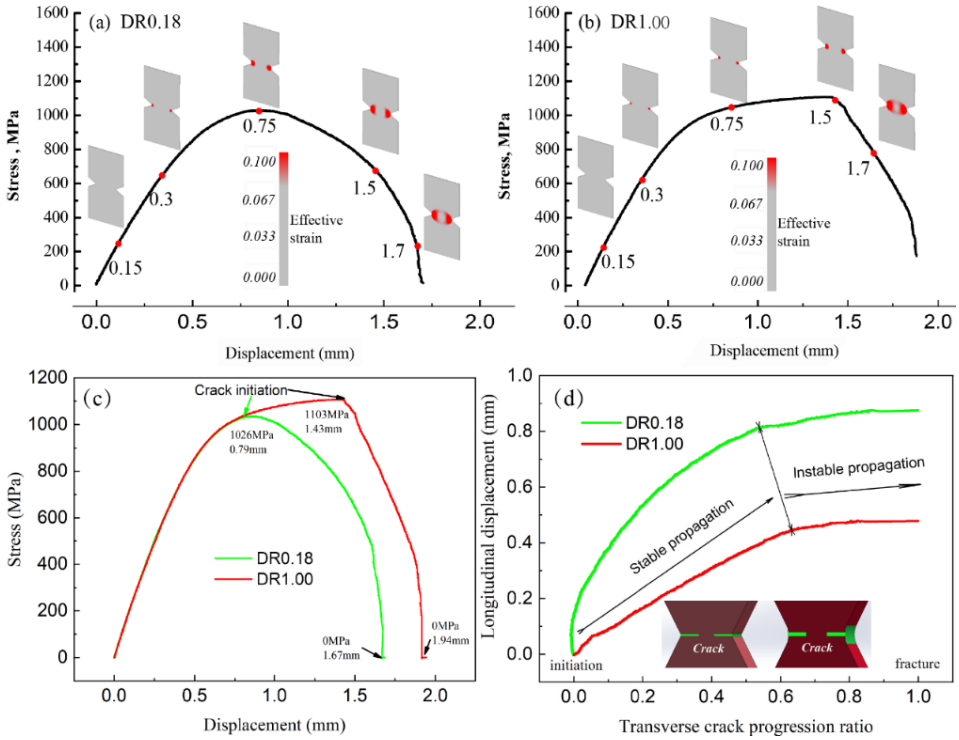


**Figure 2.** (**a**–**c**) Engineering stress versus axial displacement curves of DEN tension on Q&P steels with evolution of plastic zone at notches of R = 0.18 mm and R = 1.00 mm and (**d**) longitudinal displacement versus transverse crack progression ratio curves after initiation of cracks in DEN tension.

After reaching ultimate tensile strength of DEN tension, tensile stress slowly decreased as displacement. Meanwhile, cracks initiated and propagated at notch roots. This was different from standard tension because there was no evident crack but necking. Therefore, the dynamic propagation could be expressed by crack propagation ratio $C_r = (\sigma_{max} - \sigma)/\sigma_{max}$. Longitudinal displacement, a function of crack propagation ratio, was $\delta_l = \delta - \delta_{max}$ (1.67 mm $\geq \delta \geq$ 0.79 mm for DR0.18; 1.94 mm $\geq \delta \geq$ 1.43 mm for DR1.00, Figure 2c). Figure 2d exhibits the longitudinal displacement versus crack propagation ratio curves of DEN tension on Q&P steels. There were three stages after reaching ultimate tensile strength of DEN tension. I-stage was initiation of crack, II-stage was stable propagation and III-stage was instable propagation. Comparatively, it can be seen that the DR1.00 reached instable propagation earlier than DR0.18, although DR1.00 had a larger displacement (1.43 mm) before initiation of crack than DR0.18 (0.79 mm). The abnormal phenomena were ascribed to the potential amount of austenite for SIMT being more in DR0.18 than that in DR1.00 (Figure 1). Subsequently, it was further revealed using EBSD observations. Wu et al. [14] found that the fracture resistance (work of fracture) of Q&P steel was effectively enhanced by the transformation of metastable austenite. The transformation was further proved to be SIMT. The volume fraction of retained austenite participated into SIMT [18] is one of the most important influencing factors on the displacement of tension in DEN, largely affected by the notch root radius.

### *3.2. Fracture Toughness*

During quasi-static loading, an abrupt decrease of load occurred after crack initiation in the Q&P steels [11]. It conventionally means unstable shear propagation before fracture. It can be seen that the DEN specimens with a notch radius of 0.18 and 1 mm have similar behavior (Figure 2c). The J-integral was calculated by Equation (1) [31]. Figure 3a shows the J-integral values independent of notch radius ρ of the DEN samples. It can be seen that there is a linear relationship between the J-integral and crack advance Δa. When linear fitting is conducted on the data, a linear relationship can be found between the J-integral values and

notch radius. The critical value of toughness Jc can be deduced through Figure 3a when the notch radius is close to zero [27]. The calculated critical Jc of DR0.18 and DR1.00 were 402.97 kJ·m$^{-2}$ and 584.11 kJ·m$^{-2}$, respectively. As the notch root radius in Figure 3b is increased, Jc steadily increases for the samples with different notch root radii. It reflects the high crack sensitivity of Q&P steels. Conventionally, fracture toughness for a steel should be stable [17–25]. It means that Jc was only a relative value reflecting cracking resistance.

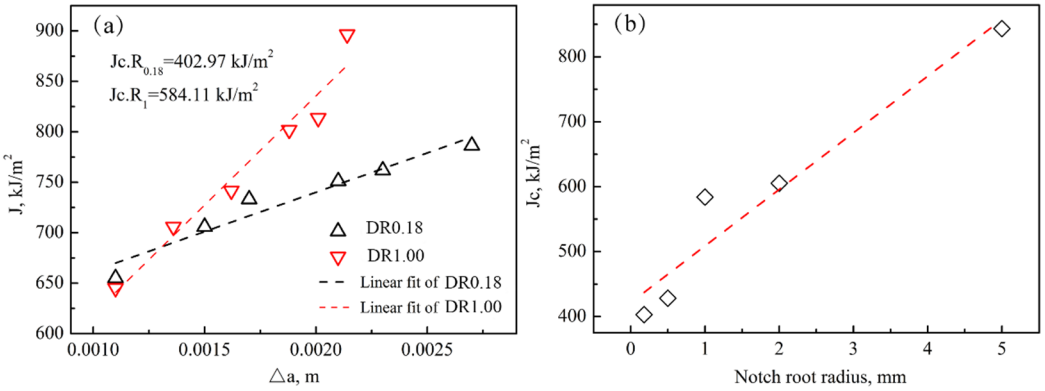


**Figure 3.** The J-integral as a function of crack advance Δa (**a**), and fracture toughness Jc in relation to notch root radius ρ (**b**).

### *3.3. TRIP Effect*

Figure 4 shows the EBSD observations of phase constituents during DEN tension of DR1.00. Figure 4a,b is the initial state before deformation, while Figure 4c,d is the final state after fracture. The volume fractions of RA (magnetic method) as a function of axial displacement are plotted in Figure 4e. It should be noted that the magnetic method for measurement of RA was conducted on sites of the crack front of the DEN specimens (Section 2.2). It can be seen that the level of RA decreases more dramatically as displacement in DEN tension of DR0.18, and the transformation rate of RA in DR1 was slower than that of DR0.18. It shows it is basically in line with the predictions using the Olson–Cohen model [32].

The level of SIMT martensite, $f_{\alpha'}$, can be calculated using the Olson–Cohen law [32],

$$f_{\alpha'} = 1 - \exp(-\beta[1 - \exp(-\alpha\varepsilon)]^n) \quad (2)$$

$$\begin{cases} \alpha = A_2^{\alpha} + \frac{A_1^{\alpha} - A_2^{\alpha}}{1+\exp(\frac{T^{\alpha} - T_o^{\alpha}}{\Delta T^{\alpha}})} \\ \beta = A_2^{\beta} + \frac{A_1^{\beta} - A_2^{\beta}}{1+\exp(\frac{T^{\beta} - T_o^{\beta}}{\Delta T^{\beta}})} \end{cases} \quad (3)$$

$\alpha$, $\beta$ are temperature and composition dependent, the coefficients used for the determination of $\alpha$, $\beta$ using Olson–Cohen parameters.

The initial microstructure contained 8 vol. % of RA (Figure 4b,e). However, DR0.18 shows an evident decrease of RA when the displacement is below 0.5 mm, and the level of RA is about 2.8% in Figure 4e. It can be deduced that the transformed austenite was mainly a filmy type, which had not been revealed by EBSD because of its thin thickness (20~100 nm) as observed by Zhu et al. [33]. However, most blocky austenite was retained after displacement to 0.5 mm. It reflects that blocky austenite apparently has high mechanical stability [34].

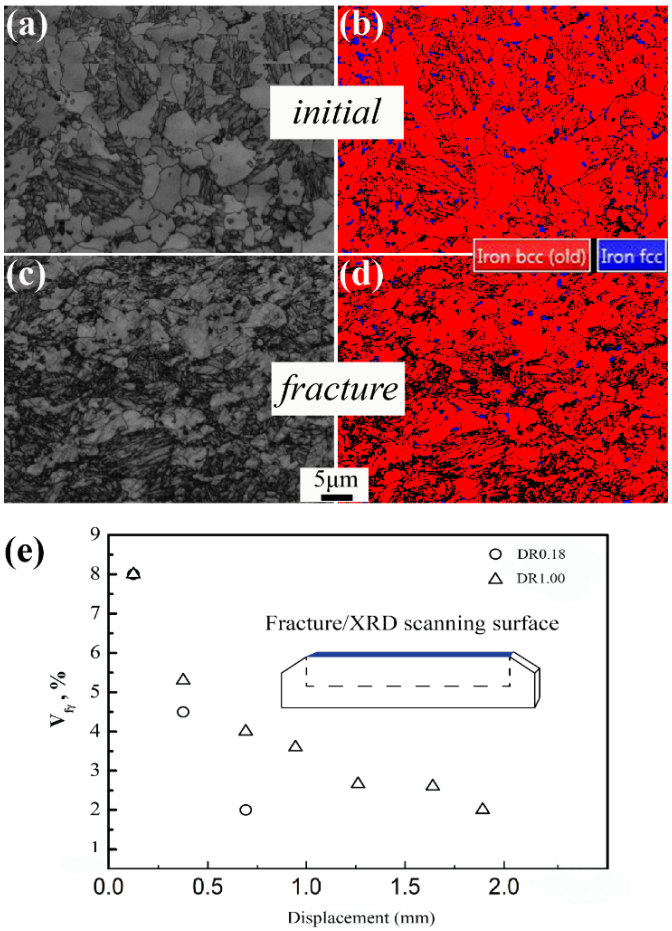


**Figure 4.** EBSD observations of phase constituents during DEN tension of DR1.00. initial state (**a**,**b**), fracture (**c**,**d**), band contrast map (**a**,**c**) and phase map (**b**,**d**). Volume fraction of RA in DR0.18 and DR1.00 (**e**).

### *3.4. SIMT Effect*

RA was proved to improve the fracture toughness by blocking the crack propagation (BCP) effect [34]. Crack propagation through martensite would be impeded upon RA, and further loading the cracks would branch out; the BCP effect stems from the toughening effect by martensitic transformation of RA [35,36]. In tension of the DEN specimens, fracture toughness of Q&P steel was effectively enhanced by the SIMT of RA in PDZs (Figures 3 and 4). Figure 5 shows the SEM and TEM observations of microvoids at notch front tip sites. Figure 5a,b show the ferrite–austenite microvoids in DR1. Figure 5c,d show the TEM observations on the propagation of microvoids in DR1. It can be noticed that microvoids exist at the sites of interfaces between martensite and ferrite (Figure 5c,d) before growing across the ferrite grain. Martensite (LM in Figure 5c, a1 and a2 in Figure 5d), as a "hard" phase, plays a vital role in impeding crack propagation in both steels. In this case, good compatibility of phase boundaries is required in the latter stage of strain. Although the nucleation possibilities of three kinds of microvoids (ferrite–ferrite, ferrite–martensite and martensite–martensite) were observed to be very close, ferrite–martensite cracking progressively predominated as the strain increased.

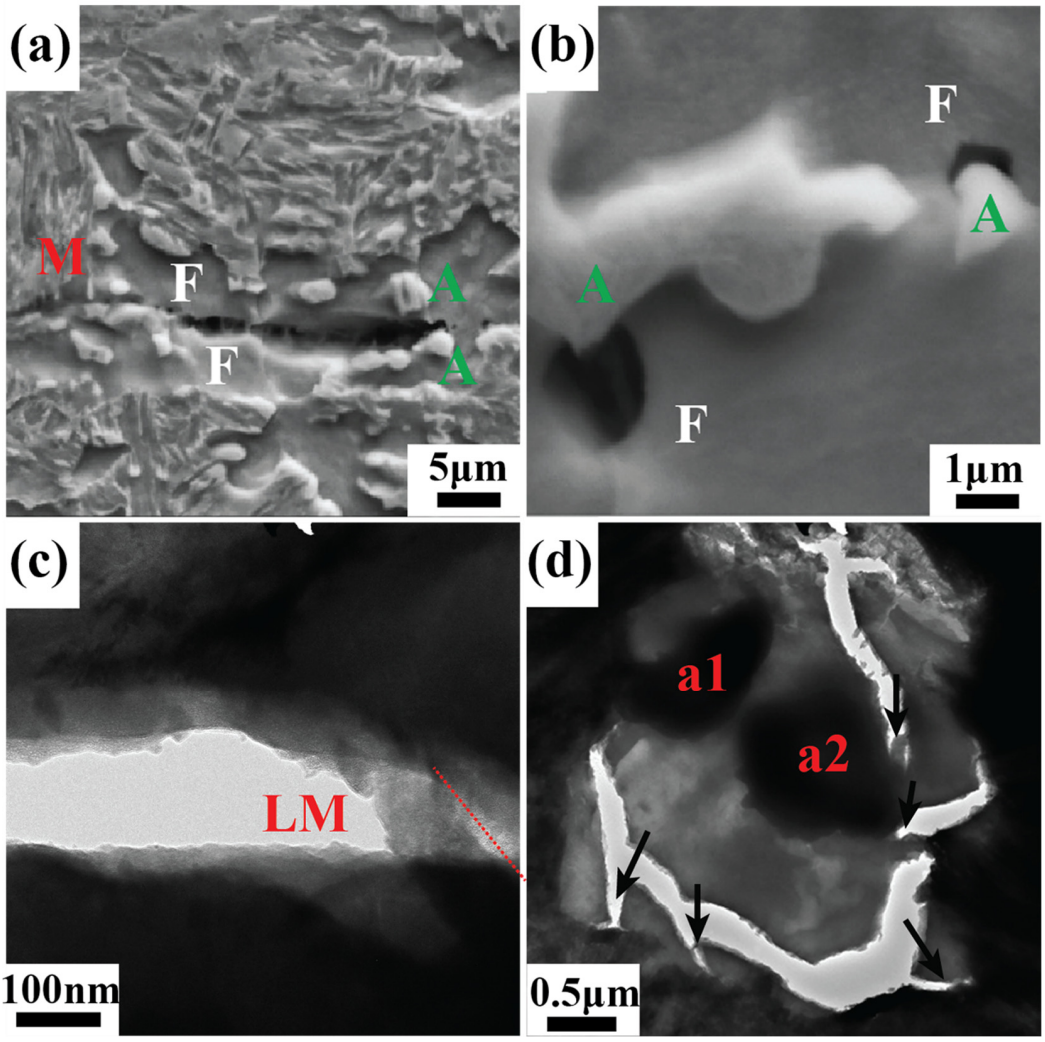


**Figure 5.** SEM (**a**,**b**) and TEM (**c**,**d**) observations of microcracks during tension of Q&P-$R_1$ steel (DEN tension with a notch root radius of 1 mm). Martensite (M), RA (A), ferrite (F) and lath martensite (LM).

Cracking resistance was related to the material's capacity to resist nucleation and growth of microvoids. Although blocky austenite mainly observed using EBSD methods in the present Q&P steel, thin, filmy type RA was observed to exist between lathy martensite [33]. The transformed austenite was mainly filmy austenite as detected by magnetic methods (Figure 4e). Morphology was a possible factor influencing the stability of austenite. Filmy austenite was considered to have high stability, not only because of adjacent hydro-stress from lath martensite, but also due to a short partitioning distance for carbon. However, the former reason was also a controversial issue [34]. It was proved that void initiation and propagation could be effectively retarded by means of the SIMT of fine RA in the narrow mixture of lath–martensite and RA [18].

Figure 6a–e shows the EBSD observation of phase constituents during tension of DR1.00 (crack advance Δa = 4 mm). The composite-like architecture of RA was located at the interface of lath–martensite in the form of nanoscale seams as marked by a white circle. This topology, as a tough barrier, might effectively impede the incoming cracks or stress/strain localizations. Figure 6d,e shows the EBSD observation of phase constituents in the vicinity of a crack during tension of DR1 (crack advance Δa = 4 mm). A macro crack was observed. It can be seen that two different orientations of RA are sandwiched by lath martensite (Figure 6d). The orientation of RA parallel to crack propagation direction was favorable to impede the crack to propagate as depicted in Figure 6g,h. Although small-angle grain boundary between martensite and filmy RA would promote crack propagation,

filmy type RA between the laths might be very active in retarding cracking (Figure 6h). However, 45 ± 3° of an angle between RA and the crack propagation direction left the filmy austenite to be untransformed (Figure 6e,h). It can be deduced that this type of austenite acted in a weak role in the SIMT effect.

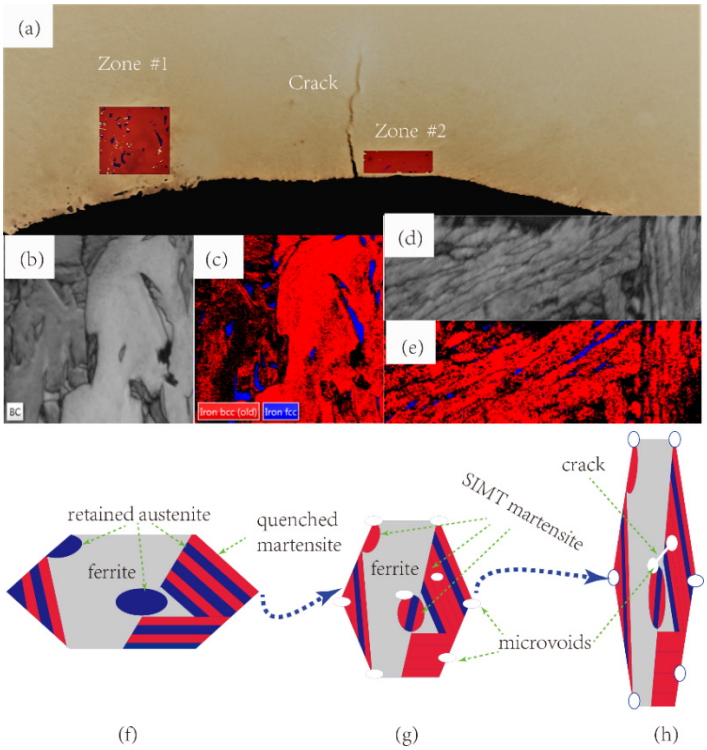


**Figure 6.** EBSD observation of phase constituents during tension of DR1.00. Crack advance Δa = 4 mm. (**a**) Notch site of the DEN specimen, (**b**,**d**) band contrast map and (**c**–**e**) phase map. Schematic diagram of evolution of microstructure during DEN tension at stages of (**f**) initial, (**g**) microvoids initiation and (**h**) crack propagation.

## 4. Conclusions

Q&P steel composed of 8 vol. % retained austenite, 61 vol. % ferrite and 31 vol. % martensite was subjected to an evaluation of the notch sensitivity and fracture toughness through tension of double edge notched specimens.

The increase rate in the plastic deformation zone modeled by a finite element method decreased with the notch root radius ρ. It demonstrated a high sensitivity of ductility and toughness in relation to notch severity.

Propagating microcracks, mostly initiated at ferrite–martensite boundaries, were proved to be effectively impeded by strain induced martensite transformation. Furthermore, electron back-scatter diffraction observations testified that favorable orientation relationship between retained austenite and propagating microcracks would largely enhance the SIMT effect of retained austenite in Q&P steels.

**Author Contributions:** R.W., writing—original draft preparation and data analysis; Y.X., microstructure observation; K.L., conceptualization, methodology, properties evaluation. All authors have read and agreed to the published version of the manuscript.

**Funding:** This research was funded by Class III Peak Discipline of Shanghai—Materials Science and Engineering (High-Energy Beam Intelligent Processing and Green Manufacturing).

**Conflicts of Interest:** The authors declare that they have no known competing financial interests or personal relationships that could have appeared to influence the work reported in this paper.

## References


1. Speer, J.; Streicher, A.; Matlock, D.; Rizzo, F.; Krauss, G.; Damm, E.; Merwin, M. *Austenite Formation and Decomposition*; TMS: Warrendale, PA, USA, 2003; pp. 505–522.
2. Hosseini, N.; Forouzan, F.; Vuorinen, E. In-situ microstructural evolution during quenching and partitioning of a high-carbon steel by high-temperature X-Ray diffraction. *Mater. Today Commun.* **2022**, *31*, 103503. [CrossRef]
3. Rong, X.; Hu, B.; Guo, H.; Enomoto, M.; Shang, C. Influence of cold rolling on the stability of retained austenite and mechanical properties of a Cu bearing low carbon low manganese steel. *Mater. Sci. Eng. A* **2022**, *850*, 143455. [CrossRef]
4. Kumar, S.; Singh, S. Microstructure-property relationship in the quenching and partitioning (Q&P) steel. *Mater. Charact.* **2023**, *196*, 112561.
5. Zhou, C.; Ye, Q.; Hu, J.; Zhao, T.; Gao, X.; Wang, Z. Ultra-high-strength multi-alloyed steel with enhanced cryogenic toughness using thermally stable retained austenite. *Mater. Sci. Eng. A* **2022**, *831*, 142356. [CrossRef]
6. Jimenez-Melero, E.; Van Dijk, N.; Zhao, L.; Sietsma, J.; Offerman, S.; Wright, J.; Van der Zwaag, S. Martensitic transformation of individual grains in low-alloyed TRIP steels. *Script. Mater.* **2007**, *56*, 421–424. [CrossRef]
7. Yang, H.; Bhadeshia, H. Austenite grain size and the martensite-start temperature. *Script. Mater.* **2009**, *60*, 493–495. [CrossRef]
8. Timokhina, I.; Hodgson, P.; Pereloma, E. Effect of microstructure on the stability of retained austenite in transformation-induced-plasticity steels. *Metall. Mater. Trans. A* **2004**, *35*, 2331–2341. [CrossRef]
9. Basuki, A.; Aernoudt, E. Influence of rolling of TRIP steel in the intercritical region on the stability of retained austenite. *J. Mater. Process. Tech.* **1999**, *89*, 37–43. [CrossRef]
10. Lee, S.; Lee, S.; De Cooman, B. Mn partitioning during the intercritical annealing of ultrafine-grained 6% Mn transformation-induced plasticity steel. *Script. Mater.* **2011**, *64*, 649–652. [CrossRef]
11. Wu, R.; Li, W.; Wang, C.; Xiao, Y.; Wang, L.; Jin, X. Stability of Retained Austenite Through a Combined Intercritical Annealing and Quenching and Partitioning (IAQP) Treatment. *Acta Metall. Sinica* **2015**, *28*, 386–393. [CrossRef]
12. De Knijf, D.; Föjer, C.; Kestens, L.; Petrov, R. Factors influencing the austenite stability during tensile testing of Quenching and Partitioning steel determined via in-situ Electron Backscatter Diffraction. *Mater. Sci. Eng. A* **2015**, *638*, 219–227. [CrossRef]
13. Socrate, S. Mechanics of Microvoid Nucleation and Growth in High-Strength Metastable Austenitic Steels. Ph. D. Thesis, MIT, Cambridge, MA, USA, 1995.
14. Wu, R.; Li, J.; Li, W.; Wu, X.; Jin, X.; Zhou, S.; Wang, L. Effect of metastable austenite on fracture resistance of quenched and partitioned (Q&P) sheet steels. *Mater. Sci. Eng. A* **2016**, *657*, 57–63.
15. Natori, M.; Song, S.; Sugimoto, K. The Effects of Fine Particle Peening on Surface Residual Stress of a TRIP-aided Bainitic Ferrite Steel. *J. Soc. Mater. Sci. Jpn.* **2014**, *63*, 662–668. [CrossRef]
16. Lacroix, G.; Pardoen, T.; Jacques, P.J. The fracture toughness of TRIP-assisted multiphase steels. *Acta Mater.* **2008**, *56*, 3900–3913. [CrossRef]
17. Srawkey, J.; Brown, W. *Fracture Toughness Testing*; Clearinghouse for Federal Scientific and Technical Information; National Aeronautics and Space Administration: Washington, DC, USA, 1965; pp. 133–136.
18. Kobayashi, J.; Ina, D.; Futamura, A.; Sugimoto, K. Fracture Toughness of an Advanced Ultrahigh-strength TRIP-aided Steel. *Isij Inter.* **2014**, *54*, 955–962. [CrossRef]
19. Qiu, H.; Wang, L.; Qi, J.; Zuo, H.; Hiraoka, K. Enhancement of fracture toughness of high-strength Cr-Ni weld metals by strain-induced martensite transformation. *Mater. Sci. Eng. A* **2013**, *579*, 71–76. [CrossRef]
20. Antolovich, S.; Chanani, G. Subcritical crack growth of TRIP steels in air under static loads. *Engin. Fract. Mech.* **1972**, *4*, 765–776. [CrossRef]
21. Mei, Z.; Morris, J. Analysis of transformation-induced crack closure. *Eng. Fract. Mech.* **1991**, *39*, 569–573. [CrossRef]
22. Sudhakar, K.; Dwarakadasa, E. A study on fatigue crack growth in dual phase martensitic steel in air environment. *Bullet. Mater. Sci.* **2000**, *23*, 193–199. [CrossRef]
23. Wang, L.; Feng, W. *Development and Application of Q&P Sheet Steels*; Advanced Steels; Springer: Berlin/Heidelberg, Germany, 2011; pp. 255–258.
24. Sugimoto, K.; Kanda, A.; Kikuchi, R.; Hashimoto, S.I.; Kashima, T.; Ikeda, S. Ductility and formability of newly developed high strength low alloy TRIP-aided sheet steels with annealed martensite matrix. *Isij Inter.* **2002**, *42*, 910–915. [CrossRef]
25. Jacques, P.; Furnémont, Q.; Pardoen, T.; Delannay, F. On the role of martensitic transformation on damage and cracking resistance in TRIP-assisted multiphase steels. *Acta Mater.* **2001**, *49*, 139–152. [CrossRef]
26. Wu, R.; Li, W.; Zhou, S.; Zhong, Y.; Wang, L.; Jin, X. Effect of Retained Austenite on the Fracture Toughness of Quenching and Partitioning (Q&P)-Treated Sheet Steels. *Metall. Mater. Trans. A* **2014**, *45*, 1892–1902.
27. Rice, J.; Sorensen, E. Continuing crack-tip deformation and fracture for plane-strain crack growth in elastic-plastic solids. *J. Mech. Phy. Solid.* **1977**, *26*, 163–186. [CrossRef]
28. van Dijk, N.; Butt, A.; Zhao, L.; Sietsma, J.; Offerman, S.; Wright, J.; van der Zwaag, S. Thermal stability of retained austenite in TRIP steels studied by synchrotron X-ray diffraction during cooling. *Acta Mater.* **2005**, *53*, 5439–5447. [CrossRef]
29. Miller, R. A Rapid X-ray Method for the Determination of Retained Austenite. *Trans. ASM* **1964**, *57*, 892–899.
30. Zhao, L.; van Dijk, N.; Brück, E.; Sietsma, J.; van der Zwaag, S. Magnetic and X-ray diffraction measurements for the determination of retained austenite in TRIP steels. *Mater. Sci. Eng. A* **2001**, *313*, 145–152. [CrossRef]

31. Li, Y.; Luo, M.; Gerlach, J.; Wierzbicki, T. Prediction of shear-induced fracture in sheet metal forming. *J. Mater. Process. Tech.* **2010**, *210*, 1858–1869. [CrossRef]
32. Samek, L.; De Moor, E.; Penning, J.; De Cooman, B. Influence of alloying elements on the kinetics of strain-induced martensitic nucleation in low-alloy, multiphase high-strength steels. *Metall. Mater. Trans. A* **2006**, *37*, 109–124. [CrossRef]
33. Zhu, X.; Li, W.; Hsu, T.; Zhou, S.; Wang, L.; Jin, X. Improved resistance to hydrogen embrittlement in a high-strength steel by quenching–partitioning-tempering treatment. *Script. Mater.* **2015**, *97*, 21–24. [CrossRef]
34. Zhou, S.B.; Hu, F.; Zhou, W.; Cheng, L.; Hu, C.Y.; Wu, K.M. Effect of retained austenite on impact toughness and fracture behavior of medium carbon submicron-structured bainitic steel. *J. Mater. Res. Tech.* **2021**, *14*, 1021–1034. [CrossRef]
35. Tu, X.; Hu, B.; Xu, R.; Guo, Q.; Luo, H. Prominent work hardening and ultrahigh yield strength both realized in 3Mn steel multiply alloyed with Cu/Ni/Al/V. *Mater. Sci. Eng. A* **2022**, *849*, 143473. [CrossRef]
36. Chhajed, B.; Mishra, K.; Singh, K.; Singh, A. Effect of prior austenite grain size on the tensile properties and fracture toughness of nano-structured bainite. *Mater. Charact.* **2022**, *192*, 112214. [CrossRef]